Composite Structures 321 (2023) 117321

Contents lists available at ScienceDirect

Composite Structures

journal homepage: www.elsevier.com/locate/compstruct

Influence of fibre cross-section profile on the multi-physical properties of uni-directional composites

Rajesh Nakka [a], A. Phanendra Kumar [a], Dineshkumar Harursampath [a,*], Sathiskumar A. Ponnusami [b,*]

[a] NMCAD Laboratory, Department of Aerospace Engineering, Indian Institute of Science, Bengaluru, Karnataka, India
[b] Aeronautics and Aerospace Research Centre, Department of Engineering, City, University of London, Northampton Square, London, United Kingdom

ARTICLE INFO

Keywords:
Fibre composites
Micro-structure
Homogenisation
Multi-physical properties

ABSTRACT

The present work comprehensively examines the influence of fibre-matrix interface perimeter on the multi-physical properties of uni-directional composite materials. Three-dimensional microstructures (containing fibres of triangular, elliptical, rectangular, C-shape and two-lobe cross-section shape) are analysed to evaluate effective thermal conduction, thermo-elastic and piezo-electric properties. Each of these properties is normalised with the respective property of RVE with circular fibre cross-section; These normalised properties are, objectively, compared with the normalised fibre cross-section perimeter (shape factor). For all the considered properties and fibre cross-sectional shapes, a novel observation is that the property experiences a drop (or rise) in the initial range of the shape factor but rises (or drops) monotonically afterwards. This is in contrast with the existing literature observations, where properties are understood to have only a monotonic increase/decrease with the shape factor. Further, it is observed that the magnitude of the initial drop (or rise) is sensitive to the fibre volume fraction and the fibre-matrix property contrast. In accordance with the literature, a strong correlation is observed among the variation of in-plane shear moduli, transverse thermal conduction and transverse dielectric constants.

1. Introduction

Composite materials have become the mainstay in various industries due to their superior specific properties compared to other engineered materials. Design and analysis of these materials are non-trivial due to the heterogeneity stemming from their construction at various length scales, spanning from ply (micro) to structural (macro) dimensions. In general, composite material properties depend on the underlying structure at lower scales, which depends on the processing parameters such as pressure, temperature, and chemical reactions used during manufacturing. For example, at the micro-scale, constituent properties and geometric features like reinforcement content, morphology and their distribution in host material control the properties at higher scales. Hence, one needs to have tight control over the processing parameters and micro-structure evolution for designing composite materials with desirable properties.

Fibre-reinforced composites (FRC) are preferred over other microstructure architectures for high-end applications due to their superior strength and stiffness along the axial direction. However, there are still challenges with FRC materials under transverse and shear loading, and active research is being conducted in this area. In this direction, the influence of using non-circular fibre cross-sections, over conventional circular cross-sections, on the composite material response has been studied widely [1–7]. Herrez et al. [4] observed increased compressive strength for the lobular-shaped fibre cross-sections. Yang et al. [5] have selected gear-shaped fibres, based on shape factors, for studying transverse stiffness and strength. It was found that gear shapes with an increased number of tips have reduced transverse stiffness and strength. XFEM-based numerical homogenisation by Higuchi et al. [6] had shown improved transverse properties for square cross-sectional shapes over circular, elliptical, two-lobed and triangular shapes. Eddie and his group have developed carbon fibres of non-circular cross-sectional shapes [8,9]. When tested alone, these fibres exhibited higher transverse modulus and strength than circular shapes. Deng et al. [10] have experimentally studied the influence of fibre cross-sectional aspect ratios using glass fibre/epoxy composites with high fibre volume fractions. Pathan et al. [11] observed that shapes with re-entrant features tend to increase stiffness but reduce damping capabilities. Sometimes the poor control over processing parameters was also found

* Corresponding authors.
E-mail addresses: rajeshnakka@iisc.ac.in (R. Nakka), attadap@iisc.ac.in (A. Phanendra Kumar), dineshkumar@iisc.ac.in (D. Harursampath), sathiskumar.ponnusami@city.ac.uk (S.A. Ponnusami).

https://doi.org/10.1016/j.compstruct.2023.117321
Received 22 March 2023; Received in revised form 26 May 2023; Accepted 1 July 2023
Available online 4 July 2023

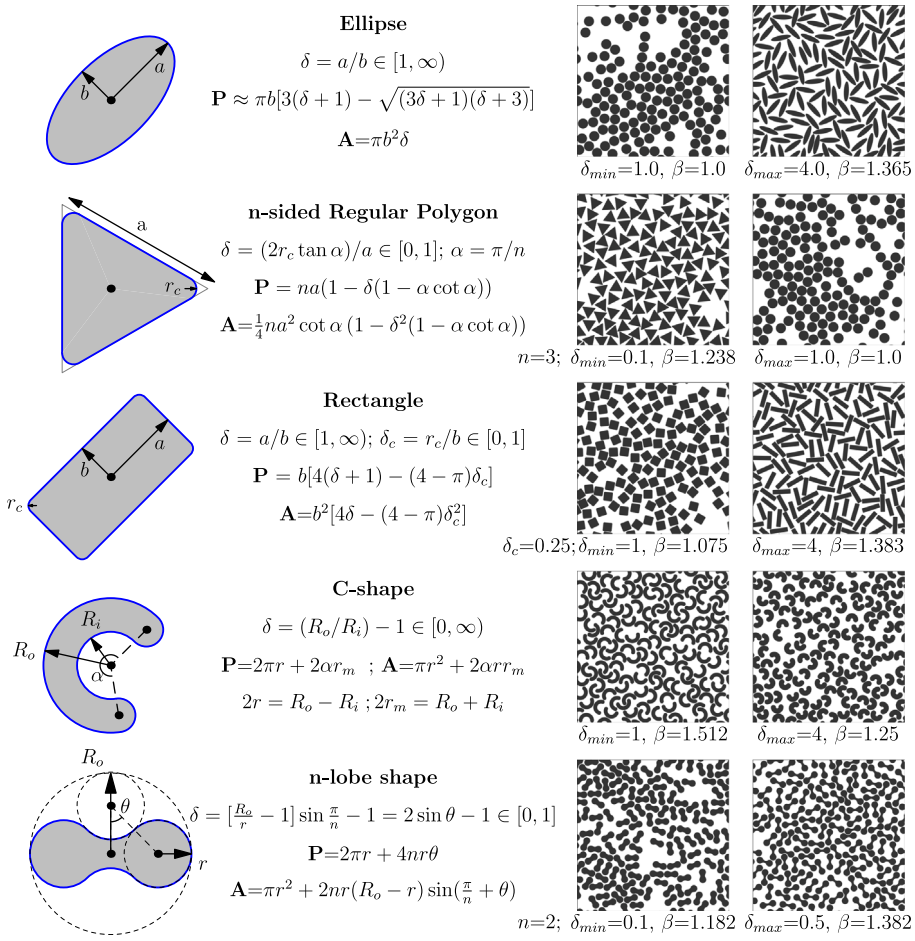

Fig. 1. Geometry of the non-circular fibre cross-sections considered in the present study and their respective representative volume elements. The parameter δ is designed to vary the perimeter of the respective shape. Note that the material axis is aligned with the fibre axis, so the fibre cross-section lies in 2–3 planes. The Ellipse perimeter is obtained from the Ramanujan approximation formula [18].

to produce non-circular cross-sections like bean [12], dog-bone or two-lobe shaped [10,13,14] non-circular fibre cross-sections. Imad Hanhan et al. [15] have observed increased stresses at higher curvature points of bean-shaped fibre cross-sections. Kaddouri et al. [16], and Shim et al. [17] have studied effective thermal conductivity dependency on the fibre cross-section wherein C and hollow shapes are found to increase the composite thermal conductivity.

The common observation of all these studies is that using non-circular shapes leads to increased contact between fibre and matrix, thus leading to better load transfer across their interface. In this work, we present interesting observations on the influence of increased fibre-matrix on 18 different composite properties using three convex and two concave non-circular shapes: ellipse, rectangle, triangle, C-shape and 2-lobe. Also, we consider 21 different geometric configurations for each shape by varying shape attributes, like aspect ratio, to get clear insights into the property variation. Further, ten different realisations are used at each geometric configuration to understand the statistical nature of the properties due to the random distribution of fibres. The shape factor, as defined in [5,14], will be used to compare the composite's response with different shapes objectively. In RVE-based numerical homogenisation, the stochastic nature of the micro-structure makes analysis dependent on the RVE size (defined as the ratio of the RVE side length to the equivalent radius of a fibre cross-section), but most of the studies have used either unit cells or smaller RVE size so properties might be affected by the RVE size.

In this study, we have chosen the RVE size as 30 following a convergence study, thus minimising the uncertainties coming from the RVE selection. Here, RVE size is a non-dimensional parameter indicating the ratio of RVE side length (in the transverse plane) to the fibre's equivalent circular cross-section radius. In total, 1050 three-dimensional RVE models are analysed under each of three different physics: thermo-elasticity, thermal conduction and piezoelectricity. Also, we investigate the influence of fibre volume fraction and constituent property contrast on the observations stemming from the analysis of RVEs containing non-circular fibre cross-sections.

The current article is organised as follows: In Section 2, RVE generation and homogenisation methods are explained, followed by the design of computational experiments. Later, the observations are presented in Section 3 for each kind of physics.

2. Methodology

The geometry of the fibre cross-section is one of the important factors that control the composite material's effective response to external loads. In general, the circular cross-section is considered in the design and analysis of FRC due to its simplicity. However, the actual fibre shape might be different from the circle due to either processing conditions [12] or deliberate design [4]. In this section, we provide the geometric details of the fibre cross-sections, followed by a method for generating RVEs containing fibres of these cross-sections and a computationally efficient homogenisation method.

2.1. Geometry of fibre cross-sections

In the present work, continuous fibre-reinforced composites are modelled, assuming a perfect interface between fibre-matrix and perfect alignment along the longitudinal direction. It is worth emphasising

that, in the current work, the simulations are conducted on three-dimensional RVEs where the fibre cross-section remains the same along its length. In this article, fibre shape implies the shape of the fibre cross-section perpendicular to its axis unless otherwise stated. From the geometry and calculus of variations, it can be proved that a circle takes the minimum perimeter for a given included area. In the case of an RVE with a constant fibre volume fraction, deviation of fibre cross-section shape from the circle leads to the increased fibre-matrix contact area. Thus, we define a shape parameter β for non-circular shapes with respect to the reference circle containing the equivalent area, $\mathbf{A}$. Let $\mathbf{P}$ be the perimeter of the non-circular shape and $\mathbf{P}^*$ be the perimeter of the reference circle, then the shape parameter β is defined as in Eq. (1).

$$\beta = \frac{\mathbf{P}}{\mathbf{P}^*} = \frac{\mathbf{P}}{\sqrt{4\pi\mathbf{A}}} \in [1, \infty) \tag{1}$$

In Fig. 1, schematics of all the five non-circular shapes (ellipse, triangle, rectangle, C-shape and 2-lobe) are listed along with their perimeter and area formulae. A parameter δ is defined for each shape to obtain different configurations of the same geometry. In the case of ellipse and rectangle, δ is their aspect ratio. For an n-sided regular polygon, δ is defined in terms of the corner radius r_c such that $\delta \to 1$ as r_c approaches the polygon's inscribed circle radius and $\delta \to 0$ as corners tend to become sharper. δ of the C-shape is defined as the width of the annular part of the C-shape normalised with the inner radius. In the case of the n-lobe shape, $\delta \in [0, 1]$ defines the minimum and maximum distance of each lobe centre from that of the whole shape centre. In other words, it is not possible to get a common tangent circle to the two successive lobes for $\delta < 0$ or $\delta > 1$. For each shape, 21 different δ values are chosen between δ_{min} and δ_{max} as shown in Fig. 1. Note that, in the case of n-sided regular polygon and n-lobular families, we chose the least possible n as it gives the maximum shape factor.

2.2. RVE generation

Periodic virtual RVEs of the microstructures containing a random distribution of fibres are generated using an optimisation-based approach developed by the authors in [19]. In this method, inclusions are placed at random locations but within the bounds of the RVE while allowing overlaps. Later, these overlaps are removed by solving a simple bound-constrained optimisation problem. One of the major difficulties in generating RVEs with non-circular or non-spherical shapes is detecting the overlap with their neighbours. To address this issue, a universal overlap detection technique [19] is developed wherein each shape is represented as a Union of n-Spheres (UnS). This simplifies overlap detection between any two similar/different shapes. Also, the randomness in fibre distribution and transverse isotropy of the generated microstructure RVEs are proved using statistical and micro-mechanical analysis [19].

In this work, fibre cross-section dimensions are evaluated using the parameter δ, see Fig. 1, such that its fibre cross-section area is equal to that of the reference circle with the radius $R_e = 2.5 \times 10^{-6}$ m. The considered δ range is split into 21 intervals for each shape, and a further ten realisations are considered at every δ. In order to ensure the RVE generation for the entire δ range, 50% fibre volume fraction V_f is considered. For each fibre cross-section shape, sample RVE images are shown for the extreme values of δ in Fig. 1. RVE size, defined as the ratio of RVE side length to the equivalent circle radius of the fibre, is selected as 30 following an RVE convergence study. Also, a constraint is imposed on the minimum distance between two fibre surfaces as 0.07 times R_e for meshing convenience in the finite element analysis (FEA) [11].

Table 1
Constitutive relations, degrees of freedom (d.o.f) at each point and considered material properties for each of the three physics. Here, $\boldsymbol{\sigma}$: stress; $\boldsymbol{C}$: elastic stiffness tensor; $\boldsymbol{\epsilon}$: strain; $\boldsymbol{\rho}$: thermal stress coefficients; $\boldsymbol{e}$: piezoelectric stress; $\boldsymbol{E}$: electric potential gradient; $\boldsymbol{D}$: electric displacements; $\boldsymbol{\kappa}$: dielectric constants; $\boldsymbol{q}$: heat flux; $\boldsymbol{K}$: thermal conductivity; $\nabla\boldsymbol{T}$: temperature gradient; u_1, u_2, u_3: displacements in directions 1, 2, 3; ϕ is electric potential; T is temperature;.

Analysis	d.o.f	Material properties
Thermo-elastic $\boldsymbol{\sigma} = \mathbf{C}\boldsymbol{\epsilon} - \boldsymbol{\rho}\Delta T$	u_1, u_2, u_3	E_{11}, E_{22}, E_{33} G_{12}, G_{13}, G_{23} $\alpha_{11}, \alpha_{22}, \alpha_{33}$
Piezo-electric $\boldsymbol{\sigma} = \mathbf{C}\boldsymbol{\epsilon} - \boldsymbol{e}\boldsymbol{E}$ $\boldsymbol{D} = \boldsymbol{e}\boldsymbol{\epsilon} - \boldsymbol{\kappa}\boldsymbol{E}$	u_1, u_2, u_3, ϕ	d_{11}, d_{21}, d_{51} $\kappa_{11}, \kappa_{22}, \kappa_{33}$
Thermal-conduction $\boldsymbol{q} = -\boldsymbol{K}\nabla\boldsymbol{T}$	T	K_{11}, K_{22}, K_{33}

2.3. Homogenisation

In this work, we are interested in evaluating the effective multi-physical properties of the microstructure represented by three-dimensional RVEs. The governing equations and the material properties of the considered three physics are summarised in Table 1.

The conventional FEA-based homogenisation [20–22] can be employed to get these properties, but it is computationally expensive wherein one needs to solve multiple load cases to get the effective material tensor along with equally demanding post-processing steps. As the number of multi-physical simulations (in total 3×1050) is relatively high, we have chosen a computationally efficient homogenisation approach based on the variational asymptotic method (VAM) [23–25], without compromising on the high-fidelity nature of the solutions. In this approach, the energy functional of the system is formulated in terms of the fluctuation fields. This energy functional is minimised to obtain the fluctuation field solution, which is further used to obtain the effective material matrix in a single simulation without any post-processing step. Also, VAM-based homogenisation inherently imposes periodic boundary conditions (PBC) to simplify the solution procedure thus ensuring a better solution (over the solutions based on kinematically uniform or statically uniform boundary conditions) for a given RVE size [20]. Its theory and finite element implementation details can be found in [23,26], so we proceed to give the final formulae for the effective material tensor, $\overline{\boldsymbol{D}}$ and effective thermal stress coefficients $\overline{\boldsymbol{\rho}} = -\overline{\boldsymbol{D}}\overline{\boldsymbol{\alpha}}$ in Eq. (2).

$$\begin{aligned}
\overline{\boldsymbol{D}} &= \frac{1}{\Omega}\left[\boldsymbol{D}_{pp} - \boldsymbol{D}_{n_a p}^T \boldsymbol{D}_{n_a n_a}^{-1} \boldsymbol{D}_{n_a p}\right] \\
\overline{\boldsymbol{\rho}} &= -\overline{\boldsymbol{D}}\overline{\boldsymbol{\alpha}} = \frac{1}{\Omega}\left[\boldsymbol{D}_{p1} - \boldsymbol{D}_{n_a p}^T \boldsymbol{D}_{n_a n_a}^{-1} \boldsymbol{D}_{n_a 1}\right]
\end{aligned} \tag{2}$$

where,

$$\begin{aligned}
\boldsymbol{D}_{n_a n_a} &= \int_\Omega \boldsymbol{B}^T \boldsymbol{D}\boldsymbol{B} d\Omega \in \mathbb{R}^{n_a \times n_a} \\
\boldsymbol{D}_{n_a p} &= \int_\Omega \boldsymbol{B}^T \boldsymbol{D} d\Omega \in \mathbb{R}^{n_a \times p} \\
\boldsymbol{D}_{pp} &= \int_\Omega \boldsymbol{D} d\Omega \in \mathbb{R}^{p \times p} \\
\boldsymbol{D}_{n_a 1} &= \int_\Omega \boldsymbol{B}^T \boldsymbol{\rho} d\Omega \in \mathbb{R}^{n_a \times 1} \\
\boldsymbol{D}_{p1} &= \int_\Omega \boldsymbol{\rho} d\Omega \in \mathbb{R}^{p \times 1}
\end{aligned} \tag{3}$$

Ω is the volume of the RVE domain, $\boldsymbol{B}$ relates field variables and their gradients, analogous to the strain–displacement matrix in mechanical loads. p is the number of rows or columns of material tensor, and n_a is the active degrees of freedom in the system. Here, active degrees of freedom (d.o.f) is obtained by excluding the d.o.f of child nodes, which follows their parent node on the opposite face/edge/vertex

Table 2
Validation of the computational tool developed in this work with the literature [24,26,28]. Here, thermo-elastic (E_{22}, G_{12}, G_{23}, α_{22}), thermal conduction (K_{22}) and Piezo-electric (d_{21}, d_{51} and κ_{22}) properties are used for the comparison.

	E_{22} (GPa)	G_{12} (GPa)	G_{23} (GPa)	$\alpha_{22}(\times 10^{-6})$
Present work	143.95	54.374	45.824	0.1946
Literature [24,26,28]	144.1	54.39	45.92	0.195
	K_{22} (W/mK)	d_{21} (C/m^2)	d_{51}(C/m^2)	κ_{22} (nC^2/Nm^2)
Present work	107.24	−0.1189	0.02073	0.1127
Literature [24,26,28]	107.45	−0.1162	0.02048	0.1106

Table 3
Material properties of the matrix and fibre, used for thermo-elastic, thermal conduction and piezoelectric analysis.

	Matrix	Fibre
Thermo-Elastic analysis	Epoxy [30]	Boron [28]
E (GPa)	3.35	379.30
ν	0.35	0.1
α ($\times 10^{-6}$/°C)	58.0	8.1
C_v (kJ/m^{3}K)	1265.0	3224.0
Thermal Conductivity	Polypropylene [28]	Carbon [28]
K (W/mK)	0.2	129.0
Piezo-Electric analysis	Epoxy [31]	PZT-7A [32]
C_{11} (GPa)	3.86	131.39
C_{12} (GPa)	2.57	82.712
C_{23} (GPa)	2.57	83.237
C_{22} (GPa)	3.86	154.837
C_{44} (GPa)	0.64	35.8
C_{55} (GPa)	0.64	25.696
d_{11} (C/m^2)	0.0	9.52183
d_{21} (C/m^2)	0.0	−2.12058
d_{51} (C/m^2)	0.0	9.349593
κ_{11} (nC^2/Nm^2)	0.0797	2.079
κ_{22} (nC^2/Nm^2)	0.0797	4.065

due to periodic boundary conditions. An in-house computational tool is developed, in *julia* language [27], for evaluating the Eq. (2). In Table 2, one can find a close match between various physical properties evaluated by this tool and the literature [24,26,28]. For this validation, we have used unit cell models as in [24,26,28] with respective fibre volume fractions and constituent properties.

3. Results and discussion

Three-dimensional models of RVEs are created with an extruded thickness of $3 \times R_e$, following the observations of [21]. Then periodic mesh is generated on these models, using an open source tool *gmsh* [29], with predominantly 8-node hexahedral elements and few (less than 2%) 6-node prism elements. Mesh convergence studies of various properties have shown microstructure effective property convergence between 200,000 and 250,000 elements. On the conservative side, we chose element sizes such that each RVE contains at least 250,000 elements. These generated finite element models are analysed under three different physics with material properties as summarised in Table 3. In all the analyses, fibre direction is chosen as 1, and 2–3 plane as the transverse cross-section.

In thermo-elastic analysis, six effective elastic moduli (E_{11}, E_{22}, E_{33}, G_{23}, G_{31} and G_{12}) and three effective thermal expansion coefficients (α_{11}, α_{22} and α_{33}) are evaluated using fibres with higher stiffness and lower thermal expansion coefficient over those of the matrix material. In order to evaluate three effective thermal conductivities (K_{11}, K_{22} and K_{33}), conductive fibres are considered in a relatively poor conductive matrix. In piezoelectric analysis, with fibre as a piezoelectric material, we have evaluated three effective piezoelectric constants (d_{11}, d_{21} and d_{51}) and effective dielectric constants (κ_{11}, κ_{22} and κ_{33}). By definition, the d_{ij} relates the influence of the applied electric field on the mechanical stresses. Under no mechanical strain, d_{11} and d_{21} are fibre directional stress (σ_{11}) and normal transverse stress (σ_{22} or σ_{33}) when an electric field is applied along the fibre direction (E_1). Similarly, d_{51} relates to in-plane shear stresses (σ_{12} and σ_{13}) when an electric field is applied in the transverse direction (E_2 and E_3).

Now, we proceed to study the variation of normalised composite properties with normalised fibre-matrix interface perimeter. As we have discussed earlier, the shape factor (β) represents the non-circular interface perimeter normalised with that of the circular interface enclosing the equal area. Composite properties with non-circular fibre cross-sections (η_{ncs}) are normalised with those due to circular fibre cross-sections (η_{cs}) of equal area, as shown in Eq. (4).

$$\widetilde{\eta} = \frac{\eta_{ncs}}{\eta_{cs}} \tag{4}$$

where η is any property of interest. For example, if a normalised property ($\widetilde{\eta}$) falls below 1 at a shape factor (β), it implies that the gain in perimeter due to non-circularity of the fibre cross-section has led to a drop in the respective composite property. As mentioned earlier, for each shape and at each shape factor, we have homogenised ten RVEs (obtained by different random spatial arrangements of fibres) to account for the statistical nature of fibre distribution. So, the mean value of the effective properties over ten different realisations is used in plotting Figs. 2 to 8. Also, one can find these mean and standard deviation values at all shape factors and for all shapes in the supplementary material.

Fibre cross-section shape influence on the longitudinal property is expected to be negligible. This is because the cumulative fibre cross-sectional area at every cross-section of the RVE along the fibre axis is constant. This results in constant average stress in the fibre, thus leading to constant modulus. The minor fluctuations in Fig. 2 are probably due to a mismatch in the Poisson's ratio of the fibre and the matrix. Accordingly, in Fig. 2(a), the variation in fibre directional properties ($\widetilde{E}_{11}$, $\widetilde{\alpha}_{11}$, $\widetilde{K}_{11}$, $\widetilde{\kappa}_{11}$ and $\widetilde{d}_{11}$) is found to be negligible (between $\pm 1\%$) for all the cross-sectional shapes and their shape factors. This observation can also be explained by the established understanding that the longitudinal directional properties can be very closely approximated with the simple rule of mixtures which depends only on the fibre volume fraction and constituent properties. On the other hand, the transverse properties depend on a few more factors, like the distribution and morphology of the fibres. So, as the microstructure is modelled with a random distribution of fibres in the present work, one can expect the transverse isotropy on the plane normal to the fibre axis. This can be observed in the very close trends for (α_{22} and α_{33}) in Fig. 2, (E_{22} and E_{33}) in Fig. 3 and (G_{12} and G_{13}, K_{22} and K_{33}, κ_{22} and κ_{33}) in Fig. 5. Now, we proceed to discuss the variation of these properties in detail.

The transverse thermal expansion coefficients, α_{22} and α_{33} as shown in Fig. 2(b) and (c), are found to have increased slightly (about 5%) in the initial range of shape factor, followed by a monotonic decrease. Here, the decreasing trend is expected due to the increased contribution of fibre whose α value is less than that of the matrix. Though the reason for the initial rise is not yet understood clearly, we show in Section 3.1 that the magnitude of the initial rise (or drop if the fibre property is higher) follows the observations made by Adam and Doner [33]. Also, as we see later, this initial drop (or rise) is observed in all the multi-physical properties but with a varied magnitude. This suggests that with the increasing fibre-matrix interface perimeter, except at its certain initial range, the contribution of the fibre to the overall properties is increasing monotonically, as in the reported literature [3,6,16].

Transverse elastic and shear moduli variation is plotted in Fig. 3 where the trend is opposite to that of the thermal expansion coefficients (α_{22} and α_{33}). Here, these properties increase up to 35% but with an initial drop which could be due to a higher fibre modulus than that of the matrix. Among the five shapes, the drop magnitude and delayed rise of property are more pronounced in the case of elliptical cross-section fibres. For the remaining shapes (Triangle, 2-lobe, rectangle and C-shape), including convex and concave shapes, the increasing

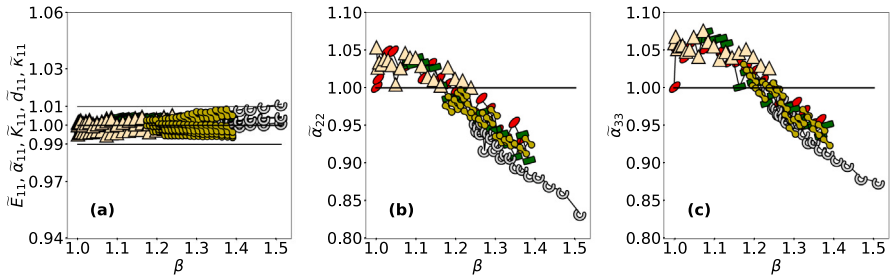

Fig. 2. The variation of normalised longitudinal effective properties ($\widetilde{E}_{11}$, $\widetilde{\alpha}_{11}$, $\widetilde{K}_{11}$, $\widetilde{\kappa}_{11}$ and $\widetilde{d}_{11}$) and the normalised effective transverse coefficient of thermal expansions (α_{22} and α_{33}) with the shape factor, for various fibre cross-section shapes. Marker shapes indicate the respective fibre cross-section shapes.

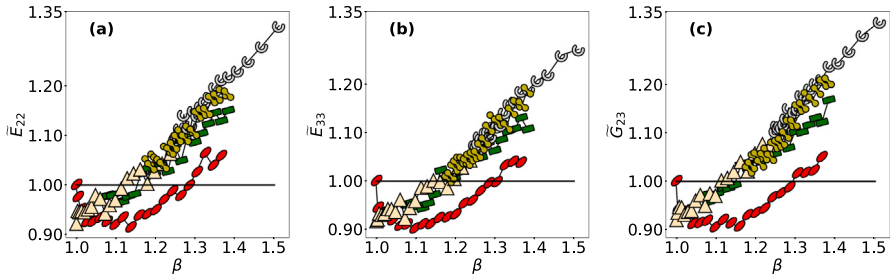

Fig. 3. The variation of normalised effective transverse elastic ($\widetilde{E}_{22}$, $\widetilde{E}_{33}$) and shear ($\widetilde{G}_{23}$) moduli of the composite with shape factor, for various fibre cross-section shapes. Marker shapes indicate the respective fibre cross-section shapes.

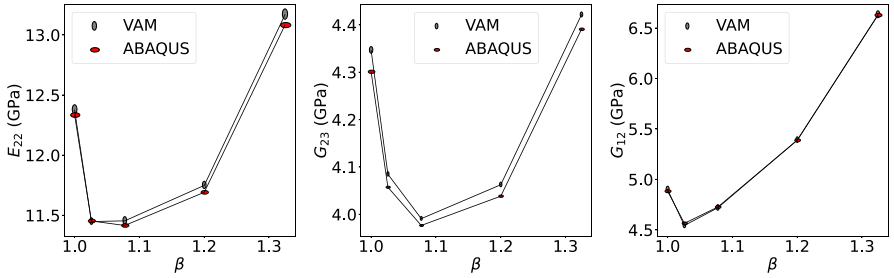

Fig. 4. Validation of elastic properties, due to elliptical fibre cross-section, obtained from VAM-based homogenisation with that obtained from conventional finite element analysis approach. Standard deviation in the respective properties over ten different realisations is indicated by the size of the markers scaled by 10^{-6}.

trend of transverse elastic property is remarkably similar across the β range. This indicates a strong correlation between the shape factor and the property variation with the fibre-matrix interface perimeter. In order to ensure that these observations are not an artefact coming from the VAM-based homogenisation tool, the same RVEs with elliptical cross-section are homogenised using a commercial finite element solver, [34], using periodic boundary conditions [20–22]. As the 3D FEA simulation in the Abaqus involves high computational costs, the validation is performed only at five aspect ratios of the elliptical cross-section but with ten different realisations at each of these aspect ratios. The mean and standard deviation of effective transverse elastic properties evaluated over ten realisations using the VAM-based and conventional FEA-based approaches are plotted in Fig. 4. The very close agreement observed in Fig. 4 gives another validation of the VAM-based homogenisation tool.

The plots of in-plane shear moduli, transverse thermal conductivity and transverse dielectric constants are plotted in Fig. 5 at one place due to their strikingly similar variation. Especially the resemblance of in-plane shear moduli G_{12} with K_{22} and G_{13} with K_{33} is noteworthy. Springer and Tsai [35] have reported this (not so intuitive) analogy wherein it was shown that the transverse thermal conductivity of uni-directional composites could be obtained using in-plane shear properties formulae given by Adams and Doner [36]. Also, one can notice a similar pattern of variation in transverse dielectric constants as in-plane shear moduli and transverse thermal conductivity. Recently, Saeed et al. [37] have reported a similar correlation between thermal conductivity and dielectric properties for wood and wood-based materials using experiments. The study [37] is intended to find thermal transmission through wood-based materials using the dielectric properties of the medium.

Note that, in Fig. 5, the initial range of β where properties are found to decrease, is relatively smaller compared to that of the transverse elastic and shear moduli (see Fig. 3). At the same time, the properties in Fig. 5 enhanced by about 50%–60% with about $\beta = 1.5$ while in Fig. 3 properties are increased by about 20%–30%. The slight fluctuations in the trends of all these plots might be due to the statistical nature of the fibre distribution. In the case of piezoelectric analysis, the piezoelectric constants d_{21} and d_{51} are also found to increase with a brief drop at the initial range of β as shown in Fig. 6. It suggests that the property d_{51} can be increased by 300% with about a 50% increase in the perimeter over that of the circle of equal area. Among all the considered properties, d_{51} has shown a significant increment suggesting that this property is very sensitive to the cross-sectional shape of the fibre.

3.1. Influence of fibre volume fraction and property contrast

We have noticed opposite variation trends for thermal expansion coefficients and the remaining properties, possibly due to opposite

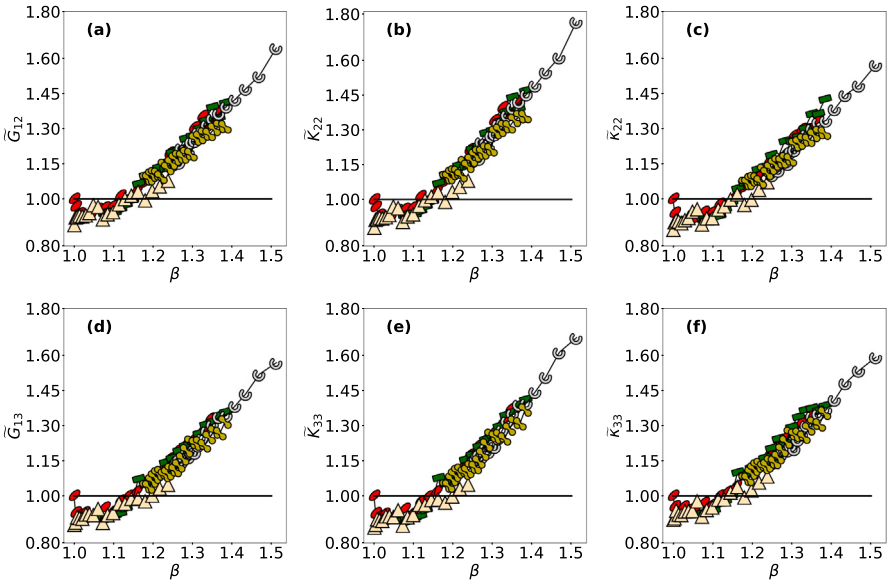

Fig. 5. The variation of normalised effective in-plane shear moduli ($\widetilde{G}_{31}$, $\widetilde{G}_{12}$), transverse thermal conductivity ($\widetilde{K}_{22}$, $\widetilde{K}_{33}$) and transverse dielectric constants ($\widetilde{\kappa}_{22}$, $\widetilde{\kappa}_{33}$) with shape factor, for various fibre cross-section shapes. Marker shapes indicate the respective fibre cross-section shapes.

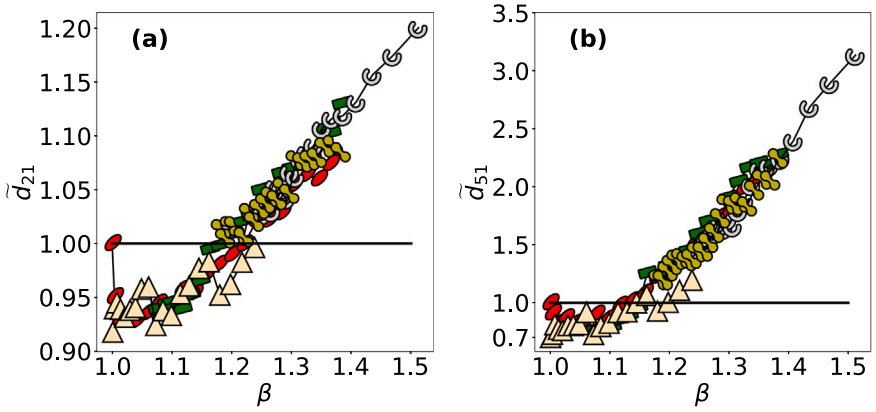

Fig. 6. The variation of normalised effective piezoelectric constants ($\widetilde{d}_{21}$) and ($\widetilde{d}_{51}$) with shape factor, for various fibre cross-section shapes. Marker shapes indicate the respective fibre cross-section shapes.

property contrasts in the fibre and matrix. To understand this phenomenon, we proceed to investigate the property variation with the constituent's property contrast and fibre volume fraction for different shape factors. For this purpose, we chose to study the elastic properties of the micro-structure with elliptical fibre cross-sections at volume fractions $V_f \in \{10\%, 30\%\}$ and fibre-matrix elastic moduli contrast $E_{cr} = E_f/E_m \in \{5, 500\}$. The transverse elastic, shear and in-plane shear moduli obtained by these combinations of V_f and E_{cr} are compared with that of $V_f = 50\%$ and $E_{cr} = 379.3/3.35 = 113.2$ (see Table 3) in Figs. 7 and 8, respectively.

In Fig. 7, the magnitude of change in the properties (E_{22}, G_{23} and G_{12}) is increasing with contrast ratio. The properties change is drastic from $E_{cr} = 5$ to $E_{cr} = 113.2$ but there is a negligible change from $E_{cr} = 113.2$ to E_{cr}=500. This is in line with the observations of Adams and Doner [33], wherein the elastic moduli increase rapidly at lower contrast ratios and stays constant from about $E_{cr} = 80$ for 50% fibre volume fraction. This hazy critical contrast ratio limit depends directly on the fibre volume fraction, with critical E_{cr} being shifted to lower values for lower values of V_f [33]. In Fig. 8, the magnitude of drop (or rise) in normalised property has increased with the fibre volume fraction. It is worth noting that the amount of drop in transverse properties is more from fibre volume fractions 30% to 50% when compared to that from 10% to 30%. This is in accordance with transverse moduli variation with V_f wherein the transverse moduli increase exponentially at higher V_f [33,36]. Hence, the influence of fibre cross-sectional shape is sensitive to the fibre volume fraction and the fibre-matrix property contrast.

3.2. Influence of inclusion distribution

In this section, we perform experiments to understand the influence of inclusion distribution on the observed jump/drop of the properties in the initial range of shape factor. For this purpose, RVEs of elliptical cross-section fibres are generated as shown in Fig. 9 wherein the aspect ratio is increased from 1 to 3 in steps of 11 while keeping the fibre cross-section centre and orientation fixed. Under these fixed centre and orientation constraints, we could generate RVEs of the fibre volume fraction V_f of about 45% with an aspect ratio of 3. So, we proceed to evaluate transverse elastic, thermal expansion and thermal conduction properties for RVEs containing elliptical inclusions with $V_f = 45\%$ and material properties as shown in Table 3. Further, at each aspect ratio, 20 realisations are considered to account for the stochastic nature of the RVE. As shown in Fig. 9(d)–(f), the effective transverse elastic properties, effective thermal expansion coefficients and the effective thermal conductivities exhibit similar drop/jump as we have observed

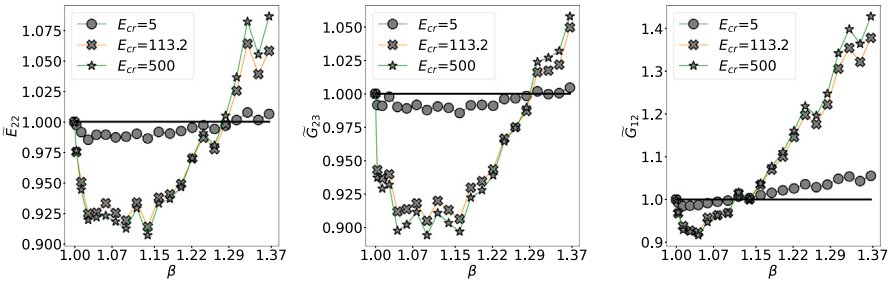

Fig. 7. Variation of elastic and shear properties with fibre-matrix elastic modulus contrast, at fibre volume fraction V_f = 50%.

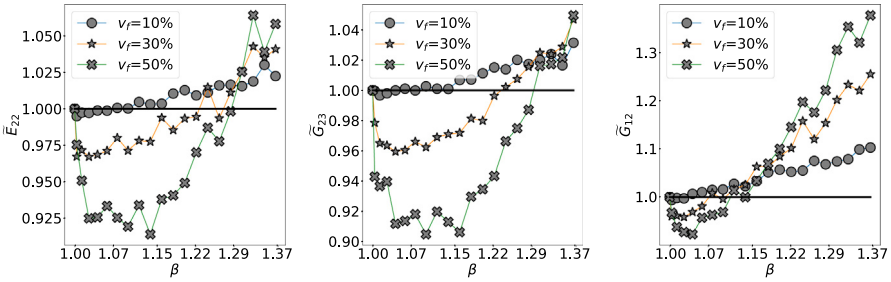

Fig. 8. Variation of elastic and shear properties with fibre volume fraction, at fibre-matrix elastic modulus contrast E_{cr} = 113.2.

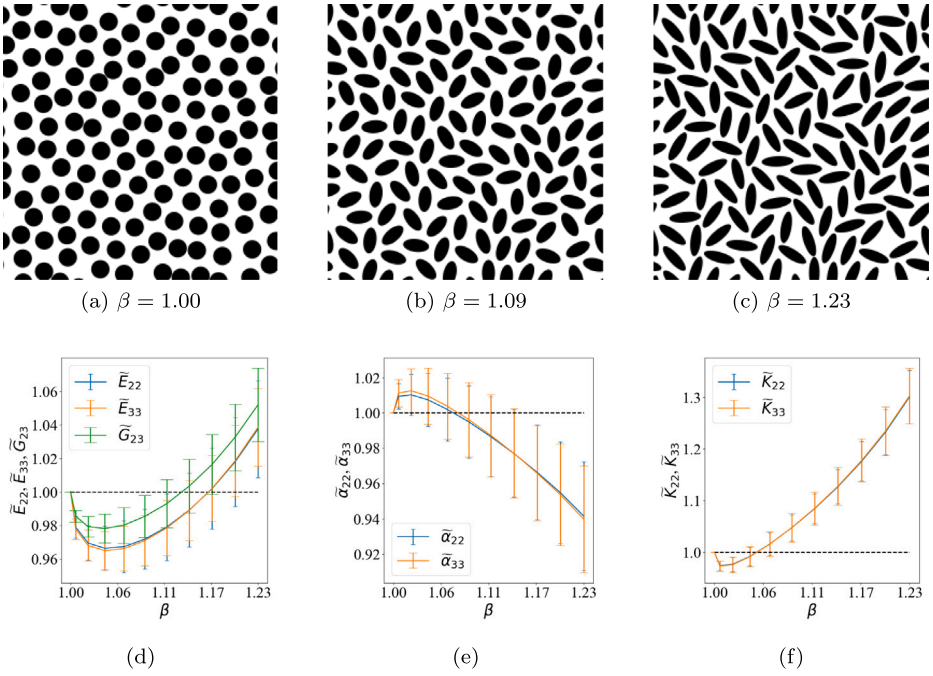

Fig. 9. (a)–(c) shows three sample RVEs with V_f = 45% showing the increased aspect ratio while keeping the centre and orientation of the ellipse fixed. (d)–(f) shows the variation of normalised transverse properties (as per Eq. (4)) with respect to the shape factor.

in Section 3. In another experiment, a unit cell with a single elliptical cross-section fibre placed at the centre is considered. The aspect ratio of this elliptical cross-section is increased continuously, and its orientation is increased from 0° to 180°. At each of these orientations and aspect ratios, effective elastic properties are evaluated and plotted in Fig. 10. These property variations show that in a range of orientation angles, the properties fall below that of the circular cross-section fibres. These two experiments suggest that the drop/jump in properties is not due to the fibre distribution in the RVE.

4. Conclusions

This study investigates the effect of the fibre cross-sectional profile, particularly the interface perimeter, for a given fibre volume fraction on the overall multi-physical properties of the uni-directional composite material. For this purpose, different microstructures containing fibres of different non-circular cross-sections (ellipse, triangle, rectangle, 2-lobe and C-shape) are considered under three different physics: thermo-elasticity, thermal conduction and piezoelectricity. Further, for each shape, 21 different perimeters and ten different realisations at each

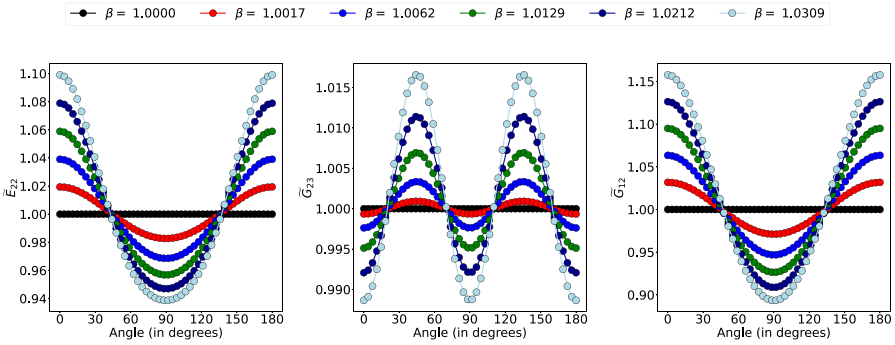

Fig. 10. Variation of the normalised effective elastic properties of a unit cell with single elliptical cross-section fibre containing 50% volume fraction. Here, the angle is the orientation of the ellipse major axis with the x-axis.

perimeter are considered to understand the statistical nature of the effective properties. Homogenisation is performed using a computationally efficient VAM-based approach to obtain effective multi-physical properties. Each of these properties is normalised with that of the micro-structure containing circular cross-section fibres. The observations while comparing the normalised properties with the normalised fibre-matrix interface perimeter (shape factor β) are listed below:

- Longitudinal properties of the composite are in-sensitive to the cross-sectional shape. This is because the longitudinal stress on the fibres remains constant irrespective of the fibre's cross-sectional shape.
- Effective transverse properties have increased (or decreased) with shape factor β, but with an initial drop (or rise) when the fibre property is higher (or lower) compared to that of the matrix. For example, effective thermal conductivity (K) of the composite with $K_{matrix} < K_{fibre}$, has decreased initially for a small range of β then increased monotonically. It suggests the increasing influence of fibre on the composite properties at higher shape factors.
- The degree of property rise (or drop) in the initial range of β is found to depend on the fibre volume fraction and the fibre-matrix property contrast. This phenomenon is more pronounced at higher fibre volume fractions and at lower property contrast values.
- Except for the transverse elastic properties of the ellipse, the trend of all properties for all shapes shows a strong correlation between the shape factor and normalised properties.
- A strong equivalence is observed among the trends of in-plane shear moduli, transverse thermal conductivity, and transverse dielectric constants, which is in line with the analytical and experimental observations by Springer and Tsai [35] and Saeed et al. [37].

In these observations, the reason for the initial drop (or rise) needs to be understood from the physics perspective and requires experimental validation. Nevertheless, this phenomenon is validated with the FEA-based homogenisation with periodic boundary conditions. In addition, the correlation among various properties as per [35,37] in Fig. 5 and fibre volume fraction and property contrast influence on properties as per [33] in Figs. 7 and 8, brings in another level of validation. Also, in future work, one needs to investigate if such an initial drop (or rise) occurs in the case of the transverse strength of fibre-reinforced composites and the multi-physical properties of the particulate composites.

CRediT authorship contribution statement

Rajesh Nakka: Conceptualization, Methodology, Software, Validation, Investigation, Formal analysis, Writing – original draft. **A. Phanendra Kumar:** Methodology, Software, Validation, Investigation, Formal analysis, Writing – original draft. **Dineshkumar Harursampath:** Supervision, Resources, Writing – review & editing. **Sathiskumar A. Ponnusami:** Supervision, Project administration, Writing – review & editing.

Declaration of competing interest

The authors declare that they have no known competing financial interests or personal relationships that could have appeared to influence the work reported in this paper.

Data availability

Data will be made available on request.

Acknowledgements

One of the authors, **Rajesh Nakka**, like to thank Dr. Abhilash M N for the insightful technical discussions.

Appendix A. Supplementary data

Supplementary material related to this article can be found online at https://doi.org/10.1016/j.compstruct.2023.117321.

References

[1] Whitney JM. Effect of fiber cross-section shape on the elastic response of composite materials. J Thermoplast Composite Mater 1994;7(4):325–43. http://dx.doi.org/10.1177/089270579400700403.
[2] Ruan X, Safari A, Chou T-W. Effective elastic, piezoelectric and dielectric properties of braided fabric composites. Composites A 1999;30(12):1435–44. http://dx.doi.org/10.1016/s1359-835x(99)00039-1.
[3] Yang L, Liu X, Wu Z, Wang R. Effects of triangle-shape fiber on the transverse mechanical properties of unidirectional carbon fiber reinforced plastics. Compos Struct 2016;152:617–25. http://dx.doi.org/10.1016/j.compstruct.2016.05.065.
[4] Herráez M, González C, Lopes C, de Villoria RG, LLorca J, Varela T, et al. Computational micromechanics evaluation of the effect of fibre shape on the transverse strength of unidirectional composites: An approach to virtual materials design. Composites A 2016;91:484–92. http://dx.doi.org/10.1016/j.compositesa.2016.02.026.
[5] Yang L, Li Z, Sun T, Wu Z. Effects of gear-shape fibre on the transverse mechanical properties of unidirectional composites: Virtual material design by computational micromechanics. Appl Compos Mater 2017;24(5):1165–78. http://dx.doi.org/10.1007/s10443-016-9580-6.
[6] Higuchi R, Yokozeki T, Nagashima T, Aoki T. Evaluation of mechanical properties of noncircular carbon fiber reinforced plastics by using XFEM-based computational micromechanics. Composites A 2019;126:105556. http://dx.doi.org/10.1016/j.compositesa.2019.105556.
[7] Kitagawa Y, Yoshimura A, Arai M, Goto K, Sugiura N. Experimental and numerical evaluation of effects of kidney-shape carbon fiber on transverse cracking of carbon fiber reinforced plastics. Composites A 2022;152:106690. http://dx.doi.org/10.1016/j.compositesa.2021.106690.
[8] Edie D, Fox N, Barnett B, Fain C. Melt-spun non-circular carbon fibers. Carbon 1986;24(4):477–82. http://dx.doi.org/10.1016/0008-6223(86)90271-x.

[9] Edie D, Dunham M. Melt spinning pitch-based carbon fibers. Carbon 1989;27(5):647–55. http://dx.doi.org/10.1016/0008-6223(89)90198-x.
[10] Deng S, Ye L, Mai Y-W. Influence of fibre cross-sectional aspect ratio on mechanical properties of glass fibre/epoxy composites I. Tensile and flexure behaviour. Compos Sci Technol 1999;59(9):1331–9. http://dx.doi.org/10.1016/s0266-3538(98)00168-7.
[11] Pathan M, Tagarielli V, Patsias S. Effect of fibre shape and interphase on the anisotropic viscoelastic response of fibre composites. Compos Struct 2017;162:156–63. http://dx.doi.org/10.1016/j.compstruct.2016.11.046.
[12] Reichanadter A, Mansson J-AE. Permeability simulation of kidney-bean shaped carbon fibers. Mater Today Commun 2022;31:103385. http://dx.doi.org/10.1016/j.mtcomm.2022.103385.
[13] Xu Z, Li J, Wu X, Huang Y, Chen L, Zhang G. Effect of kidney-type and circular cross sections on carbon fiber surface and composite interface. Composites A 2008;39(2):301–7. http://dx.doi.org/10.1016/j.compositesa.2007.10.015.
[14] Pakravan HR, Jamshidi M, Latif M, Pacheco-Torgal F. Influence of acrylic fibers geometry on the mechanical performance of fiber-cement composites. J Appl Polym Sci 2012;125(4):3050–7. http://dx.doi.org/10.1002/app.36410.
[15] Hanhan I, Sangid MD. Design of low cost carbon fiber composites via examining the micromechanical stress distributions in A42 bean-shaped versus T650 circular fibers. J Composites Sci 2021;5(11):294. http://dx.doi.org/10.3390/jcs5110294.
[16] Kaddouri W, Moumen AE, Kanit T, Madani S, Imad A. On the effect of inclusion shape on effective thermal conductivity of heterogeneous materials. Mech Mater 2016;92:28–41. http://dx.doi.org/10.1016/j.mechmat.2015.08.010.
[17] Shim H-B, Seo M-K, Park S-J. Thermal conductivity and mechanical properties of various cross-section types carbon fiber-reinforced composites. J Mater Sci 2002;37(9):1881–5. http://dx.doi.org/10.1023/a:1014959603892.
[18] Ramanujan S. Collected papers of srinivasa Ramanujan. In: AMS Chelsea publishing, Providence, RI: American Mathematical Society; 2000, p. 39, Ch. Modular equations and approximations to π.
[19] Nakka R, Harursampath D, Pathan M, Ponnusami SA. A computationally efficient approach for generating RVEs of various inclusion/fiber shapes. Compos Struct 2022;115560. http://dx.doi.org/10.1016/j.compstruct.2022.115560.
[20] Kanit T, Forest S, Galliet I, Mounoury V, Jeulin D. Determination of the size of the representative volume element for random composites: Statistical and numerical approach. Int J Solids Struct 2003;40(13–14):3647–79. http://dx.doi.org/10.1016/s0020-7683(03)00143-4.
[21] Melro A, Camanho P, Pinho S. Influence of geometrical parameters on the elastic response of unidirectional composite materials. Compos Struct 2012;94(11):3223–31. http://dx.doi.org/10.1016/j.compstruct.2012.05.004.
[22] Tian W, Qi L, Chao X, Liang J, Fu M. Periodic boundary condition and its numerical implementation algorithm for the evaluation of effective mechanical properties of the composites with complicated micro-structures. Composites B 2019;162:1–10. http://dx.doi.org/10.1016/j.compositesb.2018.10.053.
[23] Yu W, Tang T. Variational asymptotic method for unit cell homogenization of periodically heterogeneous materials. Int J Solids Struct 2007;44(11):3738–55. http://dx.doi.org/10.1016/j.ijsolstr.2006.10.020.
[24] Tang T, Yu W. Variational asymptotic micromechanics modeling of heterogeneous piezoelectric materials. Mech Mater 2008;40(10):812–24. http://dx.doi.org/10.1016/j.mechmat.2008.04.007.
[25] Pitchai P, Berger H, Guruprasad P. Investigating the influence of interface in a three phase composite using variational asymptotic method based homogenization technique. Compos Struct 2020;233:111562. http://dx.doi.org/10.1016/j.compstruct.2019.111562.
[26] Yu W, Tang T. A variational asymptotic micromechanics model for predicting thermoelastic properties of heterogeneous materials. Int J Solids Struct 2007;44(22):7510–25. http://dx.doi.org/10.1016/j.ijsolstr.2007.04.026.
[27] Bezanson J, Edelman A, Karpinski S, Shah VB. Julia: A fresh approach to numerical computing. SIAM Rev 2017;59(1):65–98. http://dx.doi.org/10.1137/141000671.
[28] Tang T, Yu W. A variational asymptotic micromechanics model for predicting conductivities of composite materials. J Mech Mater Struct 2007;2(9):1813–30.
[29] Geuzaine C, Remacle J-F. Gmsh: A 3-D finite element mesh generator with built-in pre- and post-processing facilities. Internat J Numer Methods Engrg 2009;79(11):1309–31. http://dx.doi.org/10.1002/nme.2579.
[30] Soden P, Hinton M, Kaddour A. Lamina properties, lay-up configurations and loading conditions for a range of fibre-reinforced composite laminates. Compos Sci Technol 1998;58(7):1011–22. http://dx.doi.org/10.1016/S0266-3538(98)00078-5.
[31] Kari S, Berger H, Rodriguez-Ramos R, Gabbert U. Numerical evaluation of effective material properties of transversely randomly distributed unidirectional piezoelectric fiber composites. J Intell Mater Syst Struct 2006;18(4):361–72. http://dx.doi.org/10.1177/1045389x06066293.
[32] Pettermann HE, Suresh S. A comprehensive unit cell model: A study of coupled effects in piezoelectric 1–3 composites. Int J Solids Struct 2000;37(39):5447–64. http://dx.doi.org/10.1016/S0020-7683(99)00224-3.
[33] Adams DF, Doner DR. Transverse normal loading of a unidirectional composite. J Compos Mater 1967;1(2):152–64. http://dx.doi.org/10.1177/002199836700100205.
[34] Smith M. ABAQUS/standard user's manual, version 6.9. United States: Dassault Systèmes Simulia Corp; 2009.
[35] Springer GS, Tsai SW. Thermal conductivities of unidirectional materials. J Compos Mater 1967;1(2):166–73. http://dx.doi.org/10.1177/002199836700100206.
[36] Adams DF, Doner DR. Longitudinal shear loading of a unidirectional composite. J Compos Mater 1967;1(1):4–17. http://dx.doi.org/10.1177/002199836700100102.
[37] Saeed N, Malen JA, Chamanzar M, Krishnamurti R. Experimental correlation of thermal conductivity with dielectric properties of wood and wood-based materials: Possibilities for rapid in-situ building energy evaluation. J Build Eng 2022;50:104178. http://dx.doi.org/10.1016/j.jobe.2022.104178.